

The third peak structure in the double J/ψ spectrum

Peng-Yu Niu,^{1,2} Zhenyu Zhang,^{1,2} Qian Wang,^{1,2,*} and Meng-Lin Du^{3,†}

¹Guangdong Provincial Key Laboratory of Nuclear Science, Institute of Quantum Matter,
South China Normal University, Guangzhou 510006, China

²Guangdong-Hong Kong Joint Laboratory of Quantum Matter,

Southern Nuclear Science Computing Center, South China Normal University, Guangzhou 510006, China

³School of Physics, University of Electronic Science and Technology of China, Chengdu 611731, China

(Dated: April 12, 2023)

Quantum Chromodynamics (QCD) is the fundamental theory of strong interaction, whose color confinement property allows for the existence of any color-neutral objects, i.e. the so-called hadrons. In the conventional quark model, hadrons are classified into mesons and baryons, made of quark-antiquark and three quarks, respectively. However, since the observation of the $\chi_{c1}(3872)$, a.k.a. $X(3872)$, in 2003, numerous hadrons beyond the above two configurations have been discovered, i.e. exotic hadrons. On the other hand, as unique direct measurable objects, hadrons provide a way to reveal the mystery of the nonperturbative QCD. Therefore, continuous efforts have been put forward by both experimentalists and theorists to understand the formation of hadrons, in particular exotic hadrons. Up to now, dozens of exotic candidates have been reported and most of them are in the heavy quarkonium energy region. For instance, the most famous hidden-charm pentaquarks $P_c(4312)^+$, $P_c(4440)^+$, $P_c(4457)^+$, the first doubly charmed tetraquark T_{cc}^+ , the fully charmed tetraquark $X(6900)$ and so on. A considerable portion of them have nearby S -wave thresholds and can be viewed as either hadronic molecular candidates [1] or cusp effects [2].

Among those exotic candidates, the fully heavy systems are particularly interesting due to the absence of light quarks. The LHCb [3] and CMS [4] collaboration performed a search for narrow resonances in the $\Upsilon(1S)\mu^+\mu^-$ channel around the four-bottom quark mass region. Unfortunately, no significant excess of events was observed. The situation was broken up by the LHCb collaboration [5] in 2020, which reported a narrow structure around 6.9 GeV and a broad structure in the $J/\psi J/\psi$ channel. In addition to the two structures claimed in the main text, the LHCb collaboration, in the supplementary material, also performed a fit with three Breit-Wigner (BW) lineshapes. Those three structures were reported by the CMS collaboration two years later [6]. Meanwhile, the ATLAS Collaboration also reported the existence of the $X(6900)$ in the $J/\psi\psi'$ mass spectrum in 2022 [7]. Besides the mentioned peak structures, there is also a dip around 6.75 GeV in the $J/\psi J/\psi$ invariant mass spectrum. The controversy about the structure around 7.2 GeV among the three collaborations is the key to

approaching the mystery of fully charmed tetraquarks. It is noticed that the first and the third peaks of the

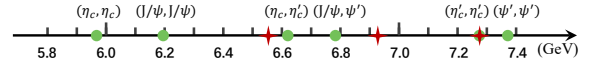


FIG. 1. (Color online) The positions of the double S -wave charmonia thresholds (green circles) below 7.4 GeV comparing with the three peak positions (red stars) from Model I in the CMS analysis [6].

CMS analysis [6] are close to the $\eta_c\eta'_c$ and $\eta'_c\eta'_c$ thresholds, respectively, ¹ as shown in Fig. 1 ². Especially, the third peak is 12 ± 20 MeV above the $\eta'_c\eta'_c$ threshold for the CMS analysis [6] and 55^{+36}_{-42} MeV below the $\eta'_c\eta'_c$ threshold for the ATLAS analysis [7]. Considering the uncertainties, they coincide with the $\eta'_c\eta'_c$ threshold as shown in Fig. 1. Therefore, to shed light on the nature of the third peak structure one cannot avoid the effect of the $\eta'_c\eta'_c$ channel. In this short communication, we aim at exploring the nature of the third peak by considering the S -wave charmonium pair in pp collision.

In the hadronic molecular picture, the production of exotic hadrons involves two ingredients, i.e. the bare production vertex and the final-state interaction. As the production of excited charmonium is smaller than that of ground charmonium, we consider the scattering among the lowest two S -wave charmonium doublets (see the supplementary material). In addition, the double pseudoscalar charmonia can couple to double vector charmonia by rearranging the charm and anticharm quarks, which is allowed by the heavy quark spin symmetry. In the heavy quark limit, the dynamics does not depend on the spin of heavy quarks, i.e. the Heavy Quark Spin Symmetry (HQSS). The S -wave potentials for the scattering among $1S$ and $2S$ charmonia with quantum numbers 0^{++} , 2^{++} can be related via HQSS ³. The production amplitude for each quantum number can be obtained by solving

¹ Here and what follows, we use η'_c and ψ' to denote the $\eta_c(2S)$ and $\psi(2S)$ charmonia, respectively.

² Although the $\Xi_{cc}^{++}\Xi_{cc}^{++}$ (7.24 GeV) and $\Xi_{cc}^{+}\Xi_{cc}^{+}$ (7.04 GeV) thresholds are also around 7.2 GeV, their productions are suppressed with comparison to that of double charmonium. In addition, their couplings to di- J/ψ are suppressed due to the annihilation of the light quark pair.

³ The HQSS breaking effect, which is considered as the higher or-

* qianwang@m.scnu.edu.cn

† du.ml@uestc.edu.cn

Lippmann-Schwinger equation (LSE). The details can be found in the supplementary material. To explore the underlying dynamics, two schemes, i.e. incoherence and coherence with the background contribution denoted as Scheme I and Scheme II, respectively, are performed as a comparison. We start from the $J^{PC} = 0^{++}$ case with the $\eta_c\eta_c$, $J/\psi J/\psi$, $\eta_c\eta'_c$, $J/\psi\psi'$, $\eta'_c\eta'_c$, $\psi'\psi'$ as the dynamical channels. The fitted results are presented in the sub-figures (a)-(c) of Fig. 2. Both the incoherent and coherent curves can well describe the broader structure around 6.5 GeV and the narrow structure around 6.9 GeV. In particular, the peak structure around 7.2 GeV in the $J/\psi J/\psi$ channel is also well described. However, this structure exhibits itself as a mild dip around 7.2 GeV in the $J/\psi\psi'$ channel, as a result of the unitarity of S-matrix. A typical example of similar behavior is the $f_0(980)$ which may exhibit as a peak or dip structure in various amplitude squares [8]. The reason that the signal of our case is not as significant as that of the $\pi\pi-K\bar{K}$ case is the large width. This pattern can also happen in the $\eta_c\eta_c$ and $\eta_c\eta'_c$ channels, i.e. a peak/dip structure in the $\eta_c\eta_c/\eta_c\eta'_c$ channel between the $\eta'_c\eta'_c$ and $\psi'\psi'$ thresholds. This behavior can be used to further confirm the origin of the third peak structure in the $J/\psi J/\psi$ spectrum.

TABLE I. The pole positions (in MeV) for Scheme-1 and Scheme-2 of the $J^{PC} = 0^{++}$ channel. Here the 1- σ statistical uncertainties are presented. The non-interference and interference fit results, i.e. Model I and Model II, of the CMS analysis [6] are listed in the last column for the comparison of our Scheme I and Scheme II, respectively.

| | poles (MeV) | notation | CMS data |
|----------|---|-----------------|-------------------|
| Scheme-1 | 5805^{+126}_{-272} | $X_1^{0^{++}}$ | $6552 \pm i62$ |
| | $(6849^{+31}_{-39}) \pm i(82^{+27}_{-20})$ | $X_2^{0^{++}}$ | $6927 \pm i61$ |
| | $(7304^{+8}_{-12}) \pm i(135^{+14}_{-12})$ | $X_3^{0^{++}}$ | $7287 \pm i47.5$ |
| Scheme-2 | 5425^{+19}_{-20} | $X_1'^{0^{++}}$ | - |
| | $(6067 \pm 6) \pm i(14 \pm 1)$ | $X_2'^{0^{++}}$ | - |
| | $(6883^{+34}_{-45}) \pm i(103^{+27}_{-22})$ | $X_3'^{0^{++}}$ | $6736 \pm i269.5$ |
| | $(7280^{+9}_{-11}) \pm i(212^{+48}_{-37})$ | $X_4'^{0^{++}}$ | $6918 \pm i93.5$ |

Although both the two schemes can describe the data very well, their pole structures, identified as bound states/resonances, are different as shown in Tab. I. Here only poles on the physical Riemann Sheet (RS) and the ones directly connected to the physical region are presented. As the $X_1^{0^{++}}$ is far away from the lowest $\eta_c\eta_c$ threshold and located on the unphysical RS as a virtual state, its effect on the physical observables is marginal. Meanwhile, the physical observables have little constraints on this pole. That is the reason why the

error of this pole is large. The $X_2^{0^{++}}$ is 66^{+31}_{-39} MeV above the $J/\psi\psi'$ threshold, leaving imprints around 6.9 GeV in the $J/\psi J/\psi$ spectrum and the threshold enhancement in the $J/\psi\psi'$ spectrum. The $X_3^{0^{++}}$ is 29^{+8}_{-12} MeV above the $\eta'_c\eta'_c$ threshold, leading to the significant structures around 7.2 GeV in the $J/\psi J/\psi$ spectrum and the mild dip structure in the $J/\psi\psi'$ spectrum. The dip structure around 6.75 GeV in the $J/\psi J/\psi$ invariant mass distribution is because of the inclusion of the dynamical $J/\psi\psi'$ channel. For the coherent case, the dip structure around 6.75 GeV is sharper than that of the incoherent case. The $X_1'^{0^{++}}$ is located on the physical sheet with hundreds of MeV below the lowest $\eta_c\eta_c$ threshold. Thus it does not deduce a pronounced structure in the lineshapes of the dynamical channels. It however may exhibit itself in the inelastic channels, for instance, the $J/\psi\mu^+\mu^-$, $\mu^+\mu^-\mu^+\mu^-$ channels, and so on. The $X_2'^{0^{++}}$ is 99 ± 6 MeV above the $\eta_c\eta_c$ threshold and 127 ± 6 MeV below to the $J/\psi J/\psi$ threshold, leading to the threshold increasing behavior in the $J/\psi J/\psi$ lineshape. The $X_4'^{0^{++}}$ is 5^{+9}_{-11} MeV above the $\eta'_c\eta'_c$ threshold and on the RS connecting to the physical one along the positive axis above the $\psi'\psi'$ threshold. It strongly couples to the $\psi'\psi'$ and the $\eta'_c\eta'_c$ channels, behaving as a peak structure in the $J/\psi J/\psi$ channel and a mild dip structure in the $J/\psi\psi'$ channel, respectively.

It has been shown that the data can be sufficiently well described by only considering the 0^{++} channel. It is not surprising that the inclusion of the 2^{++} channel in addition to the 0^{++} does not improve the fit quality significantly and would lead to uncontrolled uncertainties. As a result, in what follows we only focus on the 2^{++} channel for the comparison with the 0^{++} case. For the 2^{++} case, the dynamic channels are $J/\psi J/\psi$, $J/\psi\psi'$, $\psi'\psi'$ in the mass order. As shown by the sub-figures

TABLE II. The caption is the same as that of Tab. I but for the $J^{PC} = 2^{++}$ channel.

| | poles (MeV) | notation | CMS data |
|----------|---|-----------------|------------------|
| Scheme-1 | 5940^{+58}_{-74} | $X_1^{2^{++}}$ | $6552 \pm i62$ |
| | $(6677^{+28}_{-49}) \pm i(170^{+41}_{-39})$ | $X_2^{2^{++}}$ | $6927 \pm i61$ |
| | $(6910^{+46}_{-49}) \pm i(93^{+16}_{-9})$ | $X_3^{2^{++}}$ | $7287 \pm i47.5$ |
| Scheme-2 | 6092 ± 2 | $X_1'^{2^{++}}$ | - |
| | $(6928 \pm 6) \pm i(103 \pm 2)$ | $X_2'^{2^{++}}$ | $6918 \pm i93.5$ |

(d)-(f) of Fig. 2, the three lineshapes can also be well described by the incoherent and coherent schemes with the reduced chi-square $\chi^2/\text{d.o.f.}$ 1.08 and 1.09, respectively. The dip structure around 6.75 GeV also shows up in the lineshape due to the dynamic $J/\psi\psi'$ channel. On the contrary, the third peak structure around 7.2 GeV does not show up due to the absence of the $\eta'_c\eta'_c$ channel. Similarly, the dip structure between the $\eta'_c\eta'_c$ and the $\psi'\psi'$ threshold in the $J/\psi\psi'$ channel is also absent. The poles denoted as $X_i^{2^{++}}$ and $X_i'^{2^{++}}$ for the i th pole for the incoherent and coherent schemes, with physical

der contribution, for charm system is of the order Λ_{QCD}/m_c and neglected in the current calculation. Here Λ_{QCD} is the typical QCD nonperturbative momentum scale and m_c is the charm quark mass.

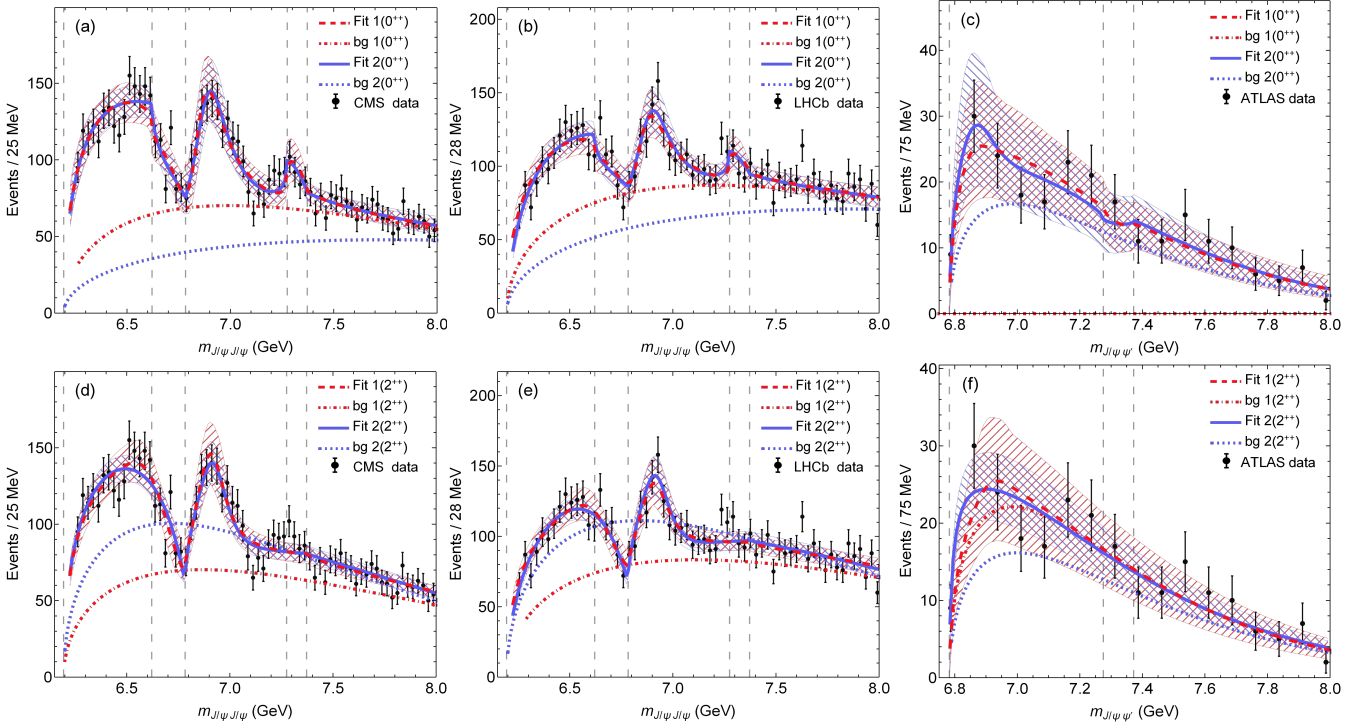


FIG. 2. (Color online) (a)-(c): The fitted double J/ψ and $J/\psi\psi'$ invariant mass distributions compared with the experimental data for the $J^{PC} = 0^{++}$ incoherent (red dashed curves and $\chi^2/\text{d.o.f} = 1.08$) and coherent (blue solid curves and $\chi^2/\text{d.o.f} = 1.00$) cases. (d)-(f): The fitting results of the $J^{PC} = 2^{++}$ with $\chi^2/\text{d.o.f} = 1.08$ and $\chi^2/\text{d.o.f} = 1.09$ for the incoherent and coherent cases, respectively. The red dot-dashed and blue dotted curves are the corresponding background contributions. The error bands (hatched areas) are 1σ uncertainty propagated from the experimental uncertainties. The vertical gray dashed lines are the thresholds of the considered dynamic channels. The experimental data are taken from the LHCb [5], CMS [6], and ATLAS [7] collaborations.

impacts are collected in Tab. II. The X_1^{2++} is located on the physical sheet and 254^{+58}_{-74} MeV below the $J/\psi J/\psi$ threshold and strongly couples to this channel. It could be viewed as a deeply $J/\psi J/\psi$ bound state. This pole is similar to the predicted $X(6200)$ of Ref. [9] and should leave a significant structure in the $\eta_c \eta_c$ channel. The X_2^{2++} has a width of hundreds of MeV, leaving it insignificant on the lineshapes. The X_3^{2++} is 127^{+46}_{-49} MeV above the $J/\psi\psi'$ threshold and accounts for the peak structure around 6.9 GeV of the $J/\psi J/\psi$ channel and the near-threshold enhancement of the $J/\psi\psi'$ channel. The $X_1'^{2++}$ strongly couples to the $J/\psi J/\psi$ channel and is 102 ± 2 MeV below the threshold, making it a $J/\psi J/\psi$ bound state. This pole contributes to the near-threshold enhancement of the $J/\psi J/\psi$ channel. The $X_2'^{2++}$ strongly couples to the $\psi'\psi'$ channel and is located on its physical sheet with 444 ± 6 MeV below the $\psi'\psi'$ threshold. This pole corresponds to the observed $X(6900)$ structure in the $J/\psi J/\psi$ channel and leads to the near-threshold increasing behavior in the $J/\psi\psi'$ channel.

From the above-mentioned four fit schemes, it is easy to see that all of them describe the data well, however, lead to different pole structures. Especially, in the 2^{++} case, neither coherent nor incoherent scheme can repro-

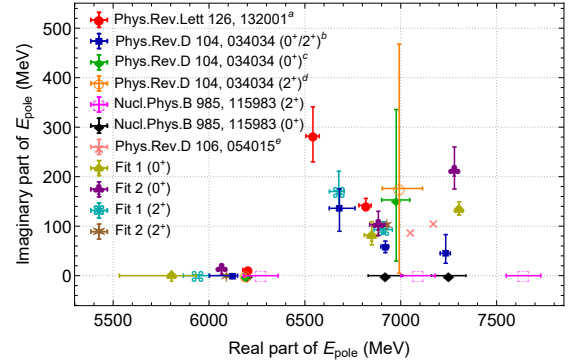


FIG. 3. (Color online) The comparison of the pole positions around 6.2 GeV, 6.9 GeV and 7.2 GeV with those from Refs. [9–12]. Our results are labeled as Fit 1 (0^+), Fit 2 (0^+), Fit 1 (2^+), and Fit 2 (2^+). The meaning of superscripts a-e is given in the context.

duce the third peak. Therefore, once future experiments confirm the third peak, it should correspond to a 0^{++} state. In addition, we also present a comparison of the

poles with others, e.g. Refs. [9–12]⁴ around 6.2 GeV, 6.9 GeV, 7.2 GeV in Fig. 3. In the literature, there are various schemes. To distinguish those schemes, the quantum numbers and the superscripts are labeled in Fig. 3. The superscript a represents the results of the $J/\psi J/\psi$ - $J/\psi\psi'$ coupled channel case of Ref. [9]. The superscript b represents the results of the $J/\psi J/\psi$ - $J/\psi\psi(2S)$ - $J/\psi\psi(3770)$ - $\psi(2S)\psi(2S)$ coupled channel case with both 0^{++} and 2^{++} quantum numbers [10]. The superscripts c and d are used to label the above four-channel case with only 0^{++} and only 2^{++} quantum numbers [10], respectively. The superscript e represents Fit-I of Ref. [12] with $\chi_{c1}\eta_c$, $\chi_{c0}\chi_{c1}$, $\chi_{c2}\chi_{c2}$ as the three dynamical channels.

In summary, we compare four schemes to shed light on the nature of the third peak structure in the $J/\psi J/\psi$ spectrum. As the $\eta'_c\eta'_c$ threshold is very close to the third peak, one cannot avoid its effect on the structure. Since the 0^{++} case has the $\eta'_c\eta'_c$ channel as one of the dynamical channels, both the incoherent and coherent cases can describe the third peak structure. This structure can also express itself as a mild dip structure in the $J/\psi\psi'$ channel between the $\eta'_c\eta'_c$ and $\psi'\psi'$ thresholds. On the contrary, the 2^{++} case does not include the $\eta'_c\eta'_c$ channel and cannot produce the third peak structure in the $J/\psi J/\psi$ channel. Thus we suggest experimentalists detailed scan both the $J/\psi J/\psi$ and the $J/\psi\psi'$ spectra, especially around 7.2 GeV to probe the nature of the third

fully charmed state. We also find that when the number of the coupled channels increases, e.g. the six-coupled-channel case for the 0^{++} channel, the predicted $X(6200)$ in Ref. [9] will become a deeper state.

Acknowledgement We are grateful to Qiang Zhao and Zhi-Hui Guo for the very helpful discussion. P. Y. N is grateful to Ji-Feng Hu for the useful discussion about the data fitting. This work is partly supported by the National Natural Science Foundation of China with Grant No. 12035007, No. 12147128, Guangdong Provincial funding with Grant No. 2019QN01X172, Guangdong Major Project of Basic and Applied Basic Research No. 2020B0301030008. Q.W. is also supported by the NSFC and the Deutsche Forschungsgemeinschaft (DFG, German Research Foundation) through the funds provided to the Sino-German Collaborative Research Center TRR110 “Symmetries and the Emergence of Structure in QCD” (NSFC Grant No. 12070131001, DFG Project-ID 196253076-TRR 110).

Author contributions Peng-Yu Niu and Zhenyu Zhang did the calculations. Meng-Lin Du and Qian Wang drafted the manuscript. All the authors made substantial contributions to the physical and technical discussions and the editing of the manuscript. All the authors have read and approved the final version of the manuscript.

-
- [1] F. K. Guo, C. Hanhart, U. G. Meißner, *et al.* Hadronic molecules. *Rev Mod Phys* 2018;90:015004.
 - [2] F. K. Guo, X. H. Liu, S. Sakai. Threshold cusps and triangle singularities in hadronic reactions. *Prog Part Nucl Phys* 2020;112:103757.
 - [3] LHCb Collaboration, R. Aaij, *et al.* Search for beautiful tetraquarks in the $\Upsilon(1S)\mu^+\mu^-$ invariant-mass spectrum. *JHEP* 2018;10:086.
 - [4] CMS Collaboration, A. M. Sirunyan, *et al.* Measurement of the $\Upsilon(1S)$ pair production cross section and search for resonances decaying to $\Upsilon(1S)\mu^+\mu^-$ in proton-proton collisions at $\sqrt{s} = 13$ TeV. *Phys Lett B* 2020;808:135578.
 - [5] LHCb Collaboration, R. Aaij, *et al.* Observation of structure in the J/ψ -pair mass spectrum. *Sci Bull* 2020;65:1983.
 - [6] CMS Collaboration. Observation of new structures in the $J/\psi J/\psi$ mass spectrum in pp collisions at $\sqrt{s} = 13$ TeV. (2022).
 - [7] ATLAS Collaboration. Observation of an excess of di-charmonium events in the four-muon final state with the ATLAS detector. (2022).
 - [8] H. A. Ahmed, C. W. Xiao. Study the molecular nature of σ , $f_0(980)$, and $a_0(980)$ states. *Phys Rev D* 2020;101:094034.
 - [9] X. K. Dong, V. Baru, F. K. Guo, *et al.* Coupled-Channel Interpretation of the LHCb Double- J/ψ Spectrum and Hints of a New State Near the $J/\psi J/\psi$ Threshold. *Phys Rev Lett* 2021;126:132001.
 - [10] Z. R. Liang, X. Y. Wu, D. L. Yao. Hunting for states in the recent LHCb di- J/ψ invariant mass spectrum. *Phys Rev D* 2021;104:034034.
 - [11] Z. G. Wang. Analysis of the $X(6600)$, $X(6900)$, $X(7300)$ and related tetraquark states with the QCD sum rules. *Nucl Phys B* 2022;985:115983.
 - [12] J. Z. Wang, X. Liu. Improved understanding of the peaking phenomenon existing in the new di- J/ψ invariant mass spectrum from the CMS Collaboration. *Phys Rev D* 2022;106:054015.
 - [13] R. Albuquerque, S. Narison, D. Rabetiarivony. Pseudoscalar and Vector $T_{QQ\bar{q}\bar{q}'}$ Spectra and Couplings from LSR at NLO. arXiv:2301.08199, 2023.
 - [14] R. M. Albuquerque, S. Narison, A. Rabemananjara, *et al.* Doubly-hidden scalar heavy molecules and tetraquarks states from QCD at NLO. *Phys Rev D* 2020;102:094001.

⁴ In Ref. [11], Regge trajectory for ordinary hadrons is employed for the fully charm system, which has been questioned by Refs. [13, 14], since the couplings between the radial excited

states and the interpolating currents are larger than the one of the ground state.